10

Growth Cones of Living Neurons Probed by Atomic Force Microscopy

Davide Ricci, Massimo Grattarola, and Mariateresa Tedesco

1. Introduction

A large body of recent literature describes the use of atomic force microscopy (AFM; **ref.** ***1***) for the study of living cells. These experimental findings clearly indicate that AFM is a very valuable tool for the 3D imaging of flat biological samples strongly adhering to a substrate, with a lateral resolution in between the resolutions of optical and electron microscopy. Moreover, a very relevant feature of AFM is its capability of analyzing local mechanical properties of living cells.

The expression "flat biological samples" includes layers of cells, such as epithelia ***(2,3)***, and single cells, such as fibroblasts and glia cells ***(4,5***). AFM technique, in its present state, seems to be less appropriate for globular structures, such as neuron bodies ***(6)***, and for string-like structures, such as neuron arborizations ***(7,8***). However, neuron growth cones are subcellular structures that seem to be very appropriate for AFM analysis: they are flat, highly specialized regions, which make very strong adhesion to the substrate. Moreover, the mechanical properties of these structures (i.e., the cytoskeleton local organization) are of great relevance for understanding the development of neural architectures. The potential, therefore, of micromechanical information from AFM is of particular value.

On the basis of these premises, this chapter will be devoted to a detailed report of experimental findings concerning the use of AFM to probe growth cones of chick embryo spinal cord neurons under vital conditions.

From: *Methods in Molecular Biology, vol. 242: Atomic Force Microscopy: Biomedical Methods and Applications*
Edited by: P. C. Braga and D. Ricci © Humana Press Inc., Totowa, NJ

2. Materials

1. Chick embryos (7–8 days (d) old).
2. Chick embryo extract (Gibco 16460-016).
3. Hanks' balanced salt solution (HBSS; Gibco 24020-091).
4. Bovine serum albumin (BSA; Sigma A-7030).
5. Trypsin solution 0.25% (Gibco 25050-014).
6. Trypsin inhibitor (Sigma T-6522).
7. DNAse (Deoxyribonuclease, type I; Sigma D-5025).
8. DMEM-F12 (Gibco 31331-028).
9. Fetal bovine serum (FBS; heat inactivated; Gibco 10108-157).
10. Horse serum (heat inactivated; Gibco 26050-070).
11. Poly-D-Lysine (Sigma P-7280) or Poly-L-Lysine (Sigma P-9155).
12. Stock supplement solution N-2 (Gibco 17502-048).
13. 5-Fluoro-2'-deoxyuridine antimitotic agent (Sigma F-0503).
14. Phosphate buffered saline solution (PBS; Gibco 14287-080).
15. Glutaraldehyde solution (Sigma G-6257).
16. Atomic force microscope: Park Scientific Instrument Autoprobe CP (Thermomicroscopes, Sunnyvale, CA).
17. Silicon nitride pyramidal tips on cantilevers with 0.01 N/m nominal spring constant (Thermomicroscopes, Sunnyvale, CA).
18. Dissection microscope (WILD-LEITZ).
19. Microdissection forceps (Fine Science Tools [FST] Dumon #5 biologie).
20. Forceps, large, small (FST).
21. Scissors, fine (FST).
22. Disposable conical tubes (Falcon 2170, 2195, or equivalent).
23. Disposable cell culture dishes (100 mm Ø Falcon, 35 mm Ø Falcon).
24. Phase contrast microscope (Diavert-LEITZ).
25. Thermo-controlled waterbath (37.5°C).
26. Centrifuge.
27. Glass slides.

3. Methods

The methods described below outline: (1) the neuron cell culture and sample preparation, (2) the AFM setup for imaging, (3) the acquisition of force-vs-distance and indentation curves, (4) the results obtained and their interpretation, and (5) a comparison with other techniques.

3.1. Neuron Cell Culture and Sample Preparation

3.1.1. Chick Embryo Spinal Cord Neuron Extraction

Spinal cord neurons were obtained through dissection of spinal cords from 8-d chick embryos and plated on treated cover slips. Dissected cords were minced in HBSS and enzymatically dissociated in 0.05% trypsin at 37°C for

25 min, then washed in CMF-HBSS containing 0.3% BSA, 0.005% DNAse (deoxyribonuclease, type I), and 0.025% trypsin inhibitor. After mechanical dissociation, the resulting single cells were suspended in MEM-F12 (1:1) supplemented with 5% FBS, 5% inactivated horse serum, and 5% chick embryo extract for plating on culture substrata.

3.1.2. Neuron Cell Culture and Sample Preparation for AFM Investigations

To prepare the culture substrata, glass slides were first cut to 20- × 40-mm pieces and then cleaned and sterilized (*see* **Note 1**). They were then incubated overnight in a poly-D-lysin solution (5 mg in 50 mL of distilled water), rinsed three times in distilled water, and dried in a sterile hood (*see* **Note 2**). Plating was made on the glass slides, which were then placed into plastic Petri dishes. The cultures were incubated at 37°C, 5% CO_2 (*see* **Note 3**). Two days after plating, the medium was replaced with MEM-F12 96%, horse serum 3%, 1% stock supplement solution N2. To free cultures from non-neural cells, 72 hours (h) after plating an antimitotic agent (5-fluoro-2-deoxiuridine, 10^{-6} *M*) was added to the culture medium.

3.1.3. Cell Fixation

For the purpose of comparing results obtained on living cells, fixated cells were also prepared. In this case, after keeping cells for 4 or 5 d in culture, the medium was removed and cultures were briefly rinsed with PBS. Cells were fixed for 20–30 min using 0.8% glutaraldehyde in PBS. Finally, slides were rinsed twice with PBS and dried.

3.2. AFM Setup for Imaging

3.2.1. AFM Setup

A Park Scientific Instruments Autoprobe CP (Sunnyvale, CA) AFM was used, which was equipped with a scanner tube allowing 100 µm (x, y) maximum scan size and 6 µm (z) excursion (*see* **Note 4**). All experiments were performed using cantilevers with 0.01 N/m nominal spring constant (*see* **Note 5**) and silicon nitride pyramidal tips (*see* **Note 6**).

Special care was taken to avoid contact between liquids and scanner, as this would cause permanent damage to the piezoelectric element and eventually to the high-voltage electronics. For this purpose, the top half of the microscope containing the scanner was enclosed in a polyethylene film sheet. This allows the scanner to move freely and does not interfere with the magnetic coupling of the sample holder. The cantilever chip was mounted on a chip holder that has a glass window behind the cantilever chip. To avoid air bubble formation, before mounting the chip holder into the microscope we wet the glass and cantilever chip

with buffer solution from a syringe and allowed a droplet of water to be trapped (kept in place by surface tension) between the chip and the glass window.

The sample was then taken out of the Petri dish, with a film of buffer solution allowed to remain on the surface. To overcome the difficulties of gluing a wet glass slide to the sample holder metal disk and also to overcome the limitations of the *x*–*y* table that has only a 12- × 12-mm range, we used the following method. First, we fixed a whole glass slide with cyanoacrylate glue to the metal sample holder disk, which is then placed on the scanner as usual. Second, we placed Vaseline onto this glass slide and pressed the cell-covered glass slide firmly onto it. This allowed us to easily move the sample in search of a good area for imaging and also to quickly change it (*see* **Note 7**).

3.2.2. Tip to Sample Approach Procedure

The first step is to approach the tip to the sample as usual with the stepper motor until the drop hanging from the cantilever holder assembly meets the liquid covering the sample glass slide. A meniscus is then formed and from this moment the surface of the sample can be seen through the on-axis optical microscope (*see* **Note 8**).

Tip-to-sample approach was always performed on a glass area next to the cell to be imaged, and before scanning the force setpoint was lowered to a small value (0.5 nN) to avoid cell damage.

3.2.3. AFM Settings for Imaging

Force-vs-distance curves before and after imaging were recorded routinely for cantilever deflection calibration purposes and for sample stiffness estimation. These curves have been transformed into force-vs-indentation plots, using as reference a force-vs-distance curve taken on glass during the same session. Images were taken with two simultaneous acquisition channels in the AFM: the z-piezo driving voltage and the error signal from the feedback loop. The first signal is proportional to the z-piezo displacement necessary to maintain the cantilever deflection (force) at the setpoint during scanning, whereas the second one records deviations of the cantilever deflections (hence from the set force) from the setpoint value.

To obtain imaging with higher spatial frequency resolution, we tuned the feedback loop parameters so that only the average cantilever deflection was kept near the setpoint value, allowing the system to generate a meaningful image from the error-signal channel, which has a wider frequency band ***(9)***. Typical scanning speeds were between 13 and 41 μm/s (*see* **Note 9**).

3.3. Acquisition of Force-vs-Distance and Indentation Curves

3.3.1. Force-vs-Distance Curves

Force-vs-distance curves were obtained by using the standard PSI software, which records the cantilever deflection, while driving the piezo in the z direction after a triangular wave. The software allowed us to set the wave frequency and to average the force-vs-distance curves taken consecutively at the same point. The curves corresponding to a given image were stored in a digital file (1024 points for each force curve) for further processing. The force scale for these curves was calibrated by using, as a reference substrate, the glass the cells adhered to. Because the glass did not appreciably indent under the loads applied, from the slope of the linear portion (after tip contact) of the force-vs-distance curve we derived the conversion factor from the error signal (in mV) to the cantilever deflection (in nm) and hence to the applied force (in nN), through the spring constant K of the cantilever (Force = $K \times$ cantilever deflection, nominal $K = 0.01$ N/m). This conversion factor depended on the intensity of the laser beam reflected from the backside of the cantilever and on the area of the spot on the photodiode. Therefore, for each series of curves taken in the same session, we left the laser alignment unchanged and began and finished the experiment performing a calibration curve on the glass.

3.3.2. Force-vs-Indentation Curves

When pushed against a soft sample, the tip of the AFM will indent the surface and the shape of the indentation curve (i.e., the relationship between the load applied and the tip penetration) will give information on the stiffness of the sample. The force-vs-indentation curves were calculated by using the approach portion of the force-vs-distance curves. The first step was to take a force-vs-distance curve on a naked glass portion of the sample as reference. From this curve, the coefficient of linear relationship between the z-piezo displacement and cantilever deflection was derived. From each of the force-vs-distance curves taken on the cells the calibration line was subtracted, thus obtaining the force-vs-indentation curve (*see* **Note 10**).

3.4. Results and Interpretation

3.4.1. Imaging

Figure 1 is a collage of various images (acquired in error mode) taken on the same growth cone of a spinal cord neuron adhering to a treated slide just taken out of the incubator. **Figure 1A** shows a topview rendering of the growth cone. Filamentous cytoskeletal structures are evident in the thick region

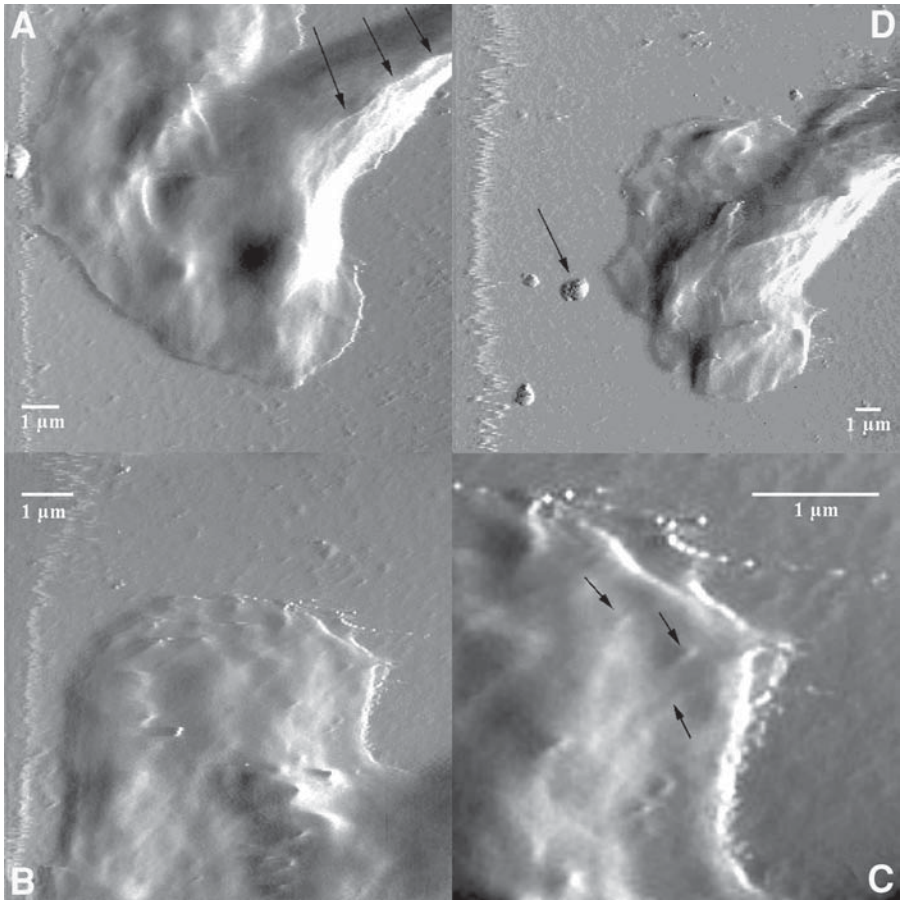

Fig. 1. Growth cone of a living spinal cord neuron adhering to a polylysine-coated glass slide. **(A)** Topview rendering of an error-mode image. Filamentous cytoskeletal structures are evident in the thick region (arrows). **(B)** Scan of the top region of the cone (partially missing in **A**). Small dot-like structures can be seen in the thick domain. **(C)** Zoom of the top right corner of the cone. A meshwork of cytoplasmic structures appears (arrows). **(D)** Image of the growth cone after about 10 min of continuous scanning. Most of the periphery of the growth cone has retracted.

(arrows). **Figure 1B** shows the top region of the cone (partially missing in **Fig. 1A**). Small dot-like structures are visible (arrows). A further zoom of the top right corner of the cone is shown in **Fig. 1C**. A meshwork of cytoplasmic structures appears (arrows). Finally, **Fig. 1D** shows the image of the growth cone after about 10 min of continuous scanning. The background globular structure on the left (arrow), present in both images, can be used to align the two images.

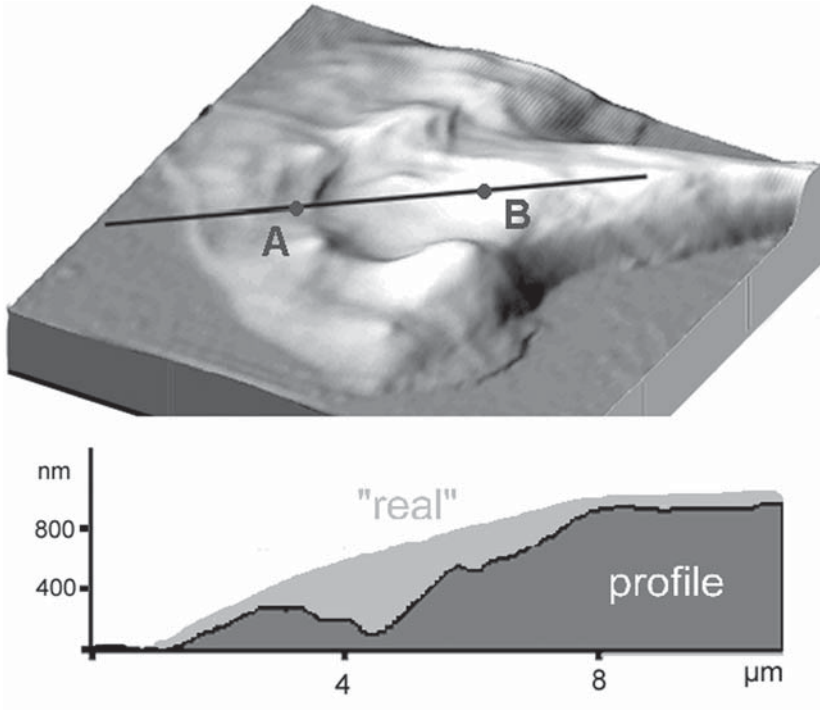

Fig. 2. 3D shaded rendering of the z-piezo signal image acquired simultaneously with the image in **Fig. 1A**, with a pictorial representation of the possible real-vs-measured profile on the growth cone.

Most of the periphery of the growth cone has clearly retracted. An increase in the relief of the filamentous structures projecting towards the neurite can be noticed. **Figure 2** shows a 3D rendering of the growth cone, as derived from the z-piezo (topographic) image (not shown), taken simultaneously with the image in **Fig. 1A**. It should be noted that the cone thickness shown in the figure is affected by the indentation of the tip on the neuron. Nevertheless, "true" thickness can be estimated and is described in **Subheading 3.4.2.** In the 3D image, a thick and a flat region can be tentatively identified, separated by a continuous relief.

Figures 3A and **B** show the growth cone of another neuron analyzed immediately after leaving the incubator. A thick tubular zone is again evident towards the neurite. Careful inspection allows one to detect a surrounding low-contrast region with flat protrusions (arrows). For comparison, **Fig. 3C** shows a similar growth cone after fixation. Similarly to **Fig. 3A**, **Fig. 3D** shows a growth cone from another living neuron, in which one can identify a thick tubular region surrounded by spiky structures (arrows).

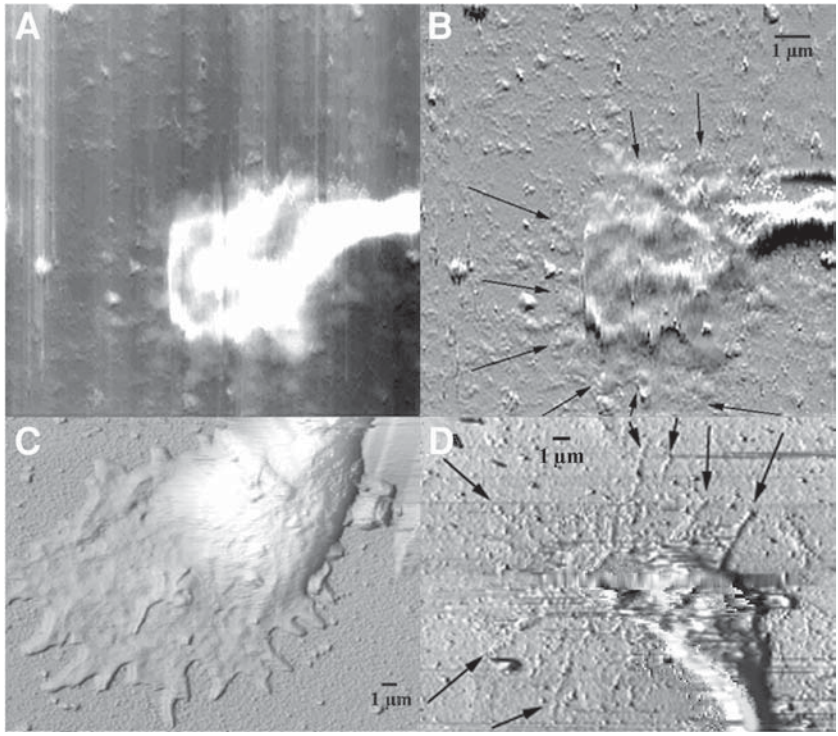

Fig. 3. Series of three images of different growth cones, in which the peripheral region has been detected by the AFM. **(A,B)** Growth cone of a living neuron analyzed immediately after leaving the incubator. A thick tubular zone is again evident. Careful inspection allows one to detect a surrounding low-contrast region with flat protrusions (arrowheads). Images obtained recording the z-piezo signal **(A)** and the error signal **(B)** simultaneously. **(C)** Image of a similar growth cone after fixation, shown for comparison. Z-piezo signal image. **(D)** Growth cone from another living neuron in which one can identify a thick tubular region surrounded by spiky structures (arrows). Image obtained recording the error signal.

Figure 4A shows a small whole neuron with several arborizations. Towards the apical end most of them seem to be disrupted. Interestingly enough, a "trace" of the borders of the arborizations is evident (**Fig. 4B** and **C**). The trace is made of small (150 nm in diameter) dot-like structures, which could be identified as clusters of adhesion molecules.

3.4.2. Indentation, Topography, and Mechanical Properties

Figure 5 shows a series of representative force-vs-indentation curves acquired upon a growth cone of a living neuron.

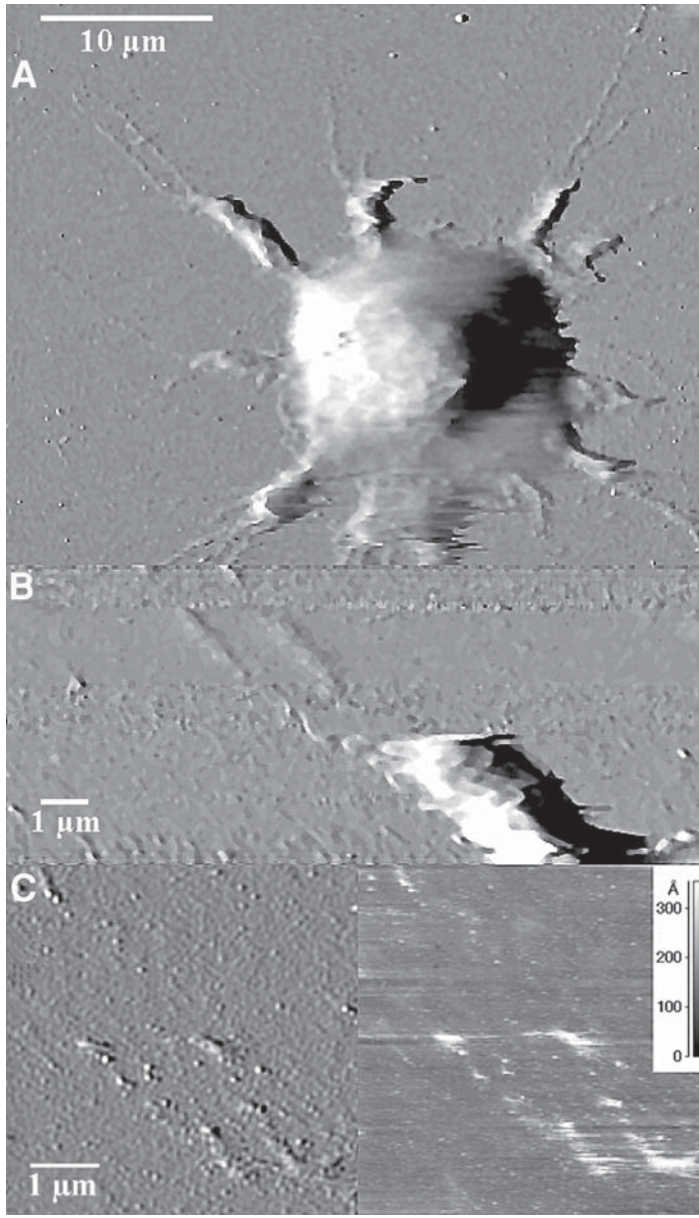

Fig. 4. **(A)** A small whole living neuron showing arborizations, imaged acquiring the error-channel signal. At the apical end most of the arborizations seem to be disrupted. **(B)** Higher magnification error-signal image of the apical end of an arborization. **(C)** Error signal and simultaneous z-piezo signal image of the same arborization apical end. The trace is made of small (approx 150 nm in diameter) dot-like structures that may be clusters of adhesion molecules.

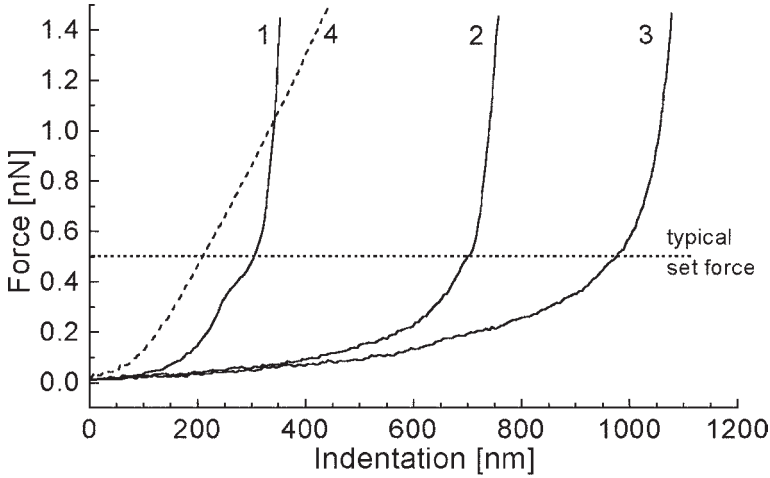

Fig. 5. Series of representative force-vs-indentation curves acquired upon a growth cone of a living neuron. Curves 1, 2, and 3 are taken moving away from the growth cone edge towards the neurite at steps of 3 μm. Each curve shows an increase in indentation with the applied force with a parabola-like behavior, until a quasivertical trend is reached. Curve 4 was taken next to the point were curve 3 was acquired but on a protrusion. A totally different trend can be observed: after an initial parabolic indentation a linear dependence on the force increase is established.

Curves 1, 2, and 3 in **Fig. 5** were taken moving away from the growth cone edge towards the neurite at steps of 3 μm and represent the typical behavior of a "soft" portion of a living cell ***(4,7)***. The indentation at first shows a parabolic-like trend followed, at higher applied forces, by a quasivertical slope. This can be explained for the first part with the classical indentation theory of a solid punch into a half space, progressively deviating from such behavior as the glass substrate contribution becomes dominant ***(10)***. The quasivertical trend with increasing force indicates that the maximum compression of the cell material has been reached and the indentation limit value attained will give an indication of the cell thickness ***(7)***. Let us now compare curves 3 and 4: curve 3 was taken onto an apparent depression of the surface, at a point like the one identified by A in **Fig. 2**, whereas curve 4 was recorded onto a stiff portion of the cell surface like the one identified by B. It is evident how in the case of curve 3 we are progressively indenting a thick portion of the cell until we reach the glass substrate, while in the second case, after a parabolic behavior for the first 100 nm of indentation, we reach a constant slope corresponding to an elastic spring constant of 0.0045 N/m. This means that, after indenting the most external "soft" cell surface, the tip interacts with submembrane structures that exhibit an elastic response ***(4)***. At the force value of 0.5 nN that corresponds to the

nominal setpoint used during imaging in the case of curve 3, we have an indentation of 950 nm, and for curve 4 we find 200 nm. We need to keep these features and figures in mind in order to understand the contrast mechanism of both the z-piezo signal and error-signal images on such specimens. This means that the deep shallows next to high peaks found in the z-piezo image cannot attributed solely to morphological features. In fact, because on thick and "soft" locations, indentations can reach the micrometer range and on stiffer ones it falls to the 100 nm range, the shallows and peaks in the "topographical" image must be essentially the result of differences in stiffness of the submembrane growth cone structure encountered by the cantilever during scanning. A pictorial representation of the possible "real"-vs-measured profile on the growth cone is shown in the second half of **Fig. 2**. Similar effects are found in the error images, where the gray scale levels represent the deviations from the feedback force (cantilever deflection) setpoint. Because the feedback loop has been tuned to give a high contrast in the error image, thus allowing temporary and relatively large deviations from the force setpoint, on the left hand side (scanning is from left to right) of an upwards slope or an increase in stiffness, the pixels will be darker, while on the right hand side they will be lighter. This can be clearly observed in **Fig. 1A**. Generally speaking, it is not possible to discriminate between a topographical change and a variation in stiffness, unless one has independent knowledge of the properties of the surface. By use of force-vs-indentation curves it is possible to discriminate the effects and estimate the thickness of the undeformed surface, at least in the point were the curve is taken. Extrapolation to similar areas can be made by an estimate of numerical values. A feature common to **Figs. 1** and **3** is a thick tubular region extending towards the neurite. The thickness of this region as read on the z-piezo image is in the order of 1 μm, to which at least 200 nm must be added to take into account indentation.

3.4.3. Identification of Growth Cone Regions

3.4.3.1. Lamellipodia

The filaments in evidence in **Fig. 1A** and **D** can be easily identified as microtubules. By comparison with images generated by the other techniques and described in the literature, the thick region can be easily identified as the so-called C domain. Note that submicrometer size structures are visible in this region. In **Figs. 1–3**, this domain is surrounded by a flat area, with thickness in the order of a few hundred nanometers. This could be identified as a lamellipodia-rich P domain.

The flat protrusions shown in **Figs. 3A** and **B** can be identified as lamellipodia structures. Their thickness is in the order of 30–60 nm. Irregulari-

ties, distortion along the scanning direction, and "islands" of biological material underline the extent of the tip–sample interaction. For comparison, **Fig. 3C** shows a similar growth cone after fixation. Lamellipodia structures with a smooth profile are now evident. The thickness is now in the 100–200-nm range: the fixation process has affected the membrane stiffness so that negligible indentation occurs during scanning.

3.4.3.2. Filopodia

The spiny protrusions surrounding the C domain in **Fig. 3D** can be identified as filopodia structures. Interestingly enough, these protrusions appear to be made of globular subunits, often arranged in a discontinuous way. These subunits have a diameter of 120–180 nm and a thickness ranging from 5 to 30 nm. They could be identified as clusters of proteins or patches of membrane adhering to the substrate, left after the tip–sample interaction. The distribution of proteins in the filopodia of growth cones is a subject of active research. Filopodia are known to be filled with bundles of actin filaments ***(11)***, and the presence of spots of tyrosine-phosphorylated proteins have been recently demonstrated at the tips of growth cones by immunofluorescence techniques ***(12)***. The formation of focal contacts by the tip of filopodia with the substrate is still an open question and further investigation of the described structures could contribute to answer it.

3.4.3.3. Arborizations

Finally, traces of discontinuous biological material are evident in the terminal regions of the arborizations of a whole neuron (**Fig. 4**). A fixed similar neuron is shown for comparison (**Fig. 6**). Here, the arborizations are smooth and continuous. The morphology of the biological details is better preserved, but no information about adhesion to the substrate can be inferred. On the contrary, we can conclude that the interaction of tip with living material does somehow affect the morphology but, at the same time, gives hints at the nanometer scale about the organization of the biological structure and about the way contact is made with the substrate.

3.5. Comparison With Other Techniques

Detailed AFM images of living flat cells, such as glia cells ***(5,6)***, fibroblasts ***(4,7)***, and epithelial cells ***(13)*** have already been analyzed in the literature. Low-resolution images of whole neurons have also been produced ***(6)***. The other available techniques for studying growth cones are as follows.

1. Whole-mount electron microscopy, which gives images with detailed information down to the nanometer ***(14)*** but on dead materials and without thickness quantification.

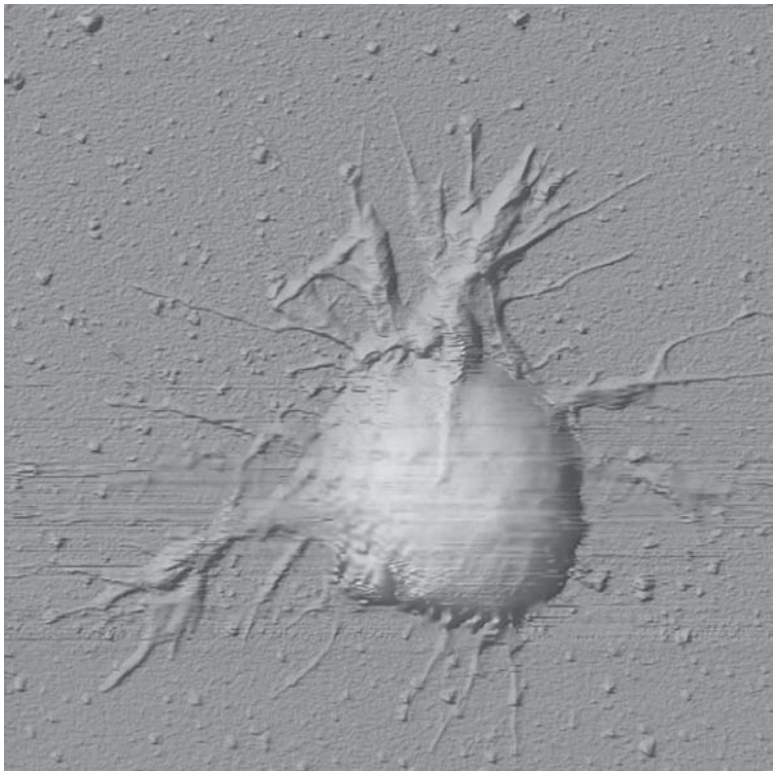

Fig. 6. A small whole fixated neuron showing arborization, to compare with the living one imaged in **Fig. 4**.

2. Fluorescence microscopy, which allows one to identify cytoskeleton components by immunofluorescence staining. Time-lapse analysis of stained (lipid probe Dioc6) living growth cones have also been described ***(15)***.
3. Video-enhanced differential interference contrast (DIC) imaging, which is widely used for generating detailed images of unstained living growth cones. This technique has allowed the identification of two distinct domains: a central, relatively thick, organelle-rich region (C domain) and a peripheral, thin, region devoid of organelles (P domain; **refs.** ***16*** and ***17***).

AFM shares with the last technique the capability of imaging unstained samples. Moreover, as compared with all the mentioned methods, it is the only one to have the potentiality of giving quantitative information on thickness. However, to put the last statement in the correct perspective, it should be underlined that any AFM-originated image of a soft sample is the result of a mechanical interaction between tip and sample. This implies indentation, and force-vs-distance curves must be used to correct the data and obtain actual

thickness. With indentation, a challenge to the adhesion of the living cone to the substrate is exerted. Finally, it is worth mentioning that, in principle, information about viscosity could also be obtained, similarly to the laser-tweezers technique ***(18)***, by carefully comparing the forward and retraction portions of the force-vs-distance curves.

4. Notes

1. Cut glass slides are used because the AFM employed for these investigations is a "scanned sample" model, able to accommodate only flat samples having maximum width of 25 mm and length of about 50 mm. When using "scanned tip" instruments, it is possible to apply the AFM directly onto the Petri dish. One advantage of using glass slides is their surface flatness with respect to Petri dishes.
2. Even if for some cell lines it is possible to grow cultures on bare substrates, for AFM investigation a good adhesion with the substrate is essential, allowing the cells to withstand the lateral forces induced by the tip during scanning
3. An advantage of using small glass slides is the possibility of preparing several samples in the Petri dish at one time that can be kept in the incubator until just before use. This allows one to increase the throughput of one single primary cell line culture both in time and number of observable cells, as usually it is not possible to maintain temperature and CO_2 control during AFM measurements. Recently, research groups have started developing systems that will allow one to control physiological environmental conditions during AFM imaging.
4. An important feature when using the AFM on living cells is the range available for the z direction in the scanner, as variations in height of several micrometers can be found during scanning. Also, x and y ranges should be several tens of micrometers.
5. Small spring constants avoid damage to the cell surface or even detachment of the cell from the substrate. We have also tried using 0.003 N/m spring constant cantilevers, but the adhesion forces between tip and sample did not result in good imaging.
6. Standard silicon nitride tips are quite sufficient for good imaging in contact mode on living cells as the visco-elasticity of the cell is the main limiting factor in resolution: in fact, a sharper tip does not improve resolution but can produce damage. Moreover, silicon nitride seems to behave better that silicon or polysilicon with respect to tip–sample adhesion.
7. A fresh supply of the buffer solution used for the culture, possibly held at 37°C, should be kept at hand, in order to be able to add it when missing.
8. An on-axis microscope is essential for positioning the tip on the sample in the required position. Either a scanned sample AFM equipped with a high magnification, long focal length microscope or a scanned tip AFM mounted onto an inverted microscope can be used. The latter obviously opens the possibility of using a wider range of optical microscopy techniques in conjunction with AFM.
9. One of the serious limitations of AFM is the low scanning speeds that have to be used on soft surfaces. A 10×10-µm image with 512 points per line is typically acquired in 8 min.

10. On the thinner portions of the cells, one observes at first the indentation process, and then a constant relationship between load and z-piezo travel is found. This means that all of the cell has been compressed and the glass surface has been "reached." One can use this last linear portion of the force-vs-distance curve to derive the coefficient and obtain the corresponding force-vs-indentation curve.

References

1. Binning, G., Quate, C. F., and Gerber, C. (1986) Atomic force microscope. *Phys. Rev. Lett.* **56,** 930–933.
2. Schoenenberger C.-A. and Hoh, J. H. (1994) Slow cellular dynamics in MDCK and R5 cells monitored by time-lapse atomic force microscopy. *Biophys. J.* **67,** 929–936.
3. Hoh, J. H. and Schoenenberger, C.-A. (1994) Surface morphology and mechanical properties of MDCK monolayers by atomic force microscopy. *J. Cell Sci.* **107,** 1105–1114.
4. Ricci, D., Tedesco, M., and Grattarola, M. (1997) Mechanical and morphological properties of living 3t6 cells probed via scanning force microscopy. *Microsc. Res. Tech.* **36,** 165–171.
5. Henderson, E., Haydon, P. G., and Sakaguchi, D. S. (1992) Actin filaments dynamics in living glial cells imaged by atomic force microscopy. *Science* **257,** 1944–1946.
6. Parpura, V., Haydon, P., and Henderson, E. (1993) Three-dimensional imaging of living neurons and glia with the atomic force microscope. *J. Cell Sci.* **104,** 427–432.
7. Ricci, D. and Grattarola M. (1994) Scanning force microscopy on live cultured cells: Imaging and force-versus-distance investigations. *J. Microsc.* **176,** 254–261.
8. Butt, H.-J., Siedle P., Seifert K., Fendler K., Seeger T., Bamberg E., et al. (1993) Scan speed limit in atomic force microscopy. *J. Microsc.* **169,** 75–84.
9. Putman, C. A. J., van der Werf. K.O., de Grooth B. G., van Hulst, N. F., Greve, J., and Hansma, P. K. (1992) A new imaging mode in atomic force microscopy based on the error signal. *Proc. SPIE.* **1639,** 198–204.
10. Sneddon, J. N. (1965) The relation between load and penetration in the axisymmetric Boussinesq problem for a punch of arbitrary profile. *Int. J. Eng. Sci.* **3,** 47–57.
11. Lewis, A. K. and Bridgam P. C. (1992) Nerve growth cone lamellipodia contain two populations of actin filaments that differ in organization and polarity. *J. Cell. Biol.* **119,** 1219–1243.
12. Da-Yu, W. and Golberg, D. J. (1993) Regulated tyrosine phosphorylation at the tips of growth cone filopodia. *J. Cell Biol.* **123,** 653–664.
13. Hoh, J. H., Sosinsky, G. E., Revel, J.-P., and Hansma, P. K. (1993) Structure of the extracellular surface of the gap junction by atomic force microscopy. *Biophys. J.* **65,** 149–163.
14. Bridgman, P. C. and Dailey M. E. (1989) The organization of myosin and actin in rapid frozen nerve growth cones. *J. Cell Biol.* **108,** 95–109.

15. Bridgman, P. C. (1991) Functional anatomy of the growth cone in relation to its role in locomotion and neurite assembly, in *The Nerve Growth Cone* (Letourneau, P. C., Kater, S. B., and Macagno E. R., eds.), Raven Press, New York, pp. 39–53.
16. Gordon-Weeks, P. R. and Mansfield G. S. (1991) Assembly of microtubules in growth cones: the role of microtubule-associated proteins, in *The Nerve Growth Cone* (Letourneau, P. C., Kater, S. B., and Macagno E. R., eds.), Raven Press, New York, pp. 55–64.
17. Goldberg, D. J., Burmeister, D. W., and Rivas, R. J. (1991) Video microscopic analysis of events in the growth cone underlying axon growth and the regulation of these events by substrate-bound proteins, in *The Nerve Growth Cone* (Letourneau, P. C., Kater, S. B., and Macagno E. R., eds.), Raven Press, New York, pp. 79–95.
18. Dai, J. and Sheetz, M. P. (1995) Mechanical properties of neuronal growth cone membranes studied by tether formation with laser optical tweezers. *Biophys. J.* **68,** 988–996.